Multiphoton Excitation and Energy Transfer Pathways in Mn^{2+}–Sulfonyl Calixarene Complexes

Constance Lecourt, Gilles Ledoux, Yan Suffren, Erwann Jeanneau, Dominique Luneau, Cédric Desroches

Dalton Transactions

ROYAL SOCIETY OF CHEMISTRY

PAPER

View Article Online
View Journal

Cite this: DOI: 10.1039/d5dt02234g

Multiphoton excitation and energy transfer pathways in Mn^{2+}–sulfonyl calixarene complexes

Constance Lecourt, [a] Gilles Ledoux, [b] Yan Suffren, [c] Erwann Jeanneau,[a] Dominique Luneau [a] and Cedric Desroches *[a]

Received 18th September 2025,
Accepted 3rd November 2025

DOI: 10.1039/d5dt02234g

rsc.li/dalton

The complexes based on Mn^{2+} ions and sulfonylcalixarene macrocycles can exhibit, when excited by blue light (360 to 400 nm), a broad luminescence band around 600 nm, resulting from the d–d transition $^4T_1(t_2g^4eg^1) \rightarrow {}^6A_1(t_2g^3eg^2)$ of the Mn^{2+} ions. A new original synthetic route to access the phenylethynyl-sulfonylcalix[4]arene macrocycle ($paThiaSO_2$) and its corresponding complexes with Mn^{2+} ions has been followed and the first experience *via* excitation with lower-energy multiphoton absorption have been realized. The results obtained demonstrate the possible two-photon sensitization of Mn^{2+} ions through the sulfonylcalixarene macrocycle.

1. Introduction

The optical properties of 3d metal coordination complexes are becoming increasingly attractive due to the abundance and low cost of these metals compared to 4d and 5d metals.[1] A large number of studies are being conducted to move away from precious metals in fields such as light-emitting diodes,[2] photocatalysts,[3] light sensors in dye-sensitized solar cells,[4] or phototherapy.[5] In recent years, there has been a growing interest in research on 3d metal coordination compounds in the field of optics. Manganese has the ability to exhibit a wide range of oxidation states. Among them, +I, +II, and +IV can display luminescence properties: for the +I state (d^6) *via* Metal-to-Ligand Charge Transfer (MLCT),[6] for the +II (d^5) state *via* metal-centered transitions (MC),[7] and for the +IV state (d^3) *via* ligand-to-metal charge transfer (LMCT).[8]

Since the beginning of the 20th century, mineral compounds based on Mn^{2+} have been used as luminescent materials. Mn(II)-doped oxides,[9] nitrides,[9] phosphates,[10] borosilicate glasse,[11,12] and sulfides[13] are considered promising candidates for the development of inexpensive and non-toxic luminescent mineral materials, used as green or red phosphors. However, it is only in recent decades that Mn(II)-based complexes with ligands such as halogenure/phosphine oxides,[14] halogenure/crown ethers,[15] and the sulfonylcalixarene macrocycle[16,17] have shown luminescent properties in both solid and solution states. In previous work, we found that under solvothermal conditions, *p-tert*-butylsulfonylcalix[4]arene mixed with a Mn^{2+} salt and fluoride forms tetranuclear metal complexes $[Mn_4(ThiaSO_2)_2F]^-$, which upon excitation at 360 nm at room temperature exhibit a strong orange eye-perceived luminescence at a wavelength of about 580 nm. This emission results from the transition between the $^4T_1(^4G)$ excited state and the $^6A_1(^6S)$ ground state of the Mn^{2+} ions present in the cluster (Fig. 1). For several years, we have continued our investigations by modifying this luminescent system to better exploit the symbiosis between the sulfonylcalixarene

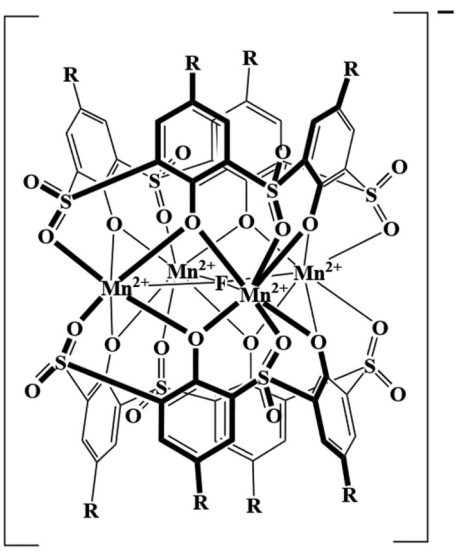

Fig. 1 Representation of tetranuclear metal anionic complexes $[Mn_4(ThiaSO_2)_2F]^-$, $ThiaSO_2$ = *p-tert*-butylsulfonylcalix[4]arene.

[a]*Universite Claude Bernard Lyon 1, CNRS, LMI UMR 5615, Villeurbanne, F-69100, France. E-mail: cedric.desroches@univ-lyon1.fr*
[b]*Univ. Lyon, Université Claude Bernard Lyon 1, CNRS, Institut Lumiere Matiere, F-69622 Villeurbanne, France*
[c]*Univ Rennes, INSA Rennes, CNRS, ISCR "Institut des Sciences Chimiques de Rennes", Rennes F-35000, France*

ligand and Mn^{2+} ions. It has been shown that the macrocycle conformation,[17,18] increasing electron delocalization along the phenolic units, as well as modulation of the counter anion[19] significantly alter the optical properties of this family of complexes in the solid-state, such as emission wavelength and oxygen sensitivity. Calix[4]arene macrocycles and their derivatives have demonstrated that the unique combination of four donor–π–acceptor (D–π–A) dipoles endows these systems with remarkable second-order Non-Linear Optical (NLO) properties.[20–23] In the cone conformation, the four phenolic units are oriented in the same direction, resulting in a hypsochromic shift of the Charge Transfer (CT) band, along with a significant increase in the second-order molecular hyperpolarizability (β). It has also been shown that the D–π–A units within calix[4]arenes do not behave entirely independently, and that the geometry of the cone, whether perfectly symmetric or pinched, affects the total dipole moment and consequently the β values. Other NLO-related properties of this family have also been reported in the literature, in particular their optical limiting capabilities, which are primarily attributed to two-photon absorption mechanisms. In this context, the thiacalix[4]arene family has emerged as particularly promising for optical limiting applications.[24] Molecular engineering efforts have led to the identification of (phenylethynyl)thiacalix[4]arenes and their derivatives as excellent candidates for such applications, based on the principle that increased electronic delocalization enhances nonlinear optical properties. Building on these findings, we investigated the ability of sulfonylcalix[4]arenes to sensitize Mn^{2+} ions *via* a two-photon absorption process. Beyond demonstrating that this family represents the first class of ligands capable of sensitizing Mn^{2+} ions through such a mechanism, this study also opens up new perspectives in the field. Furthermore, this work describes a synthetic route to access the phenylethynylsulfonylcalix[4]arene macrocycle (paThiaSO_2) and its corresponding complexes with Mn^{2+} ions.

2. Results and discussion

2.1. Synthesis

The use of the thiacalixarene macrocycle as a ligand can be achieved in two ways: (i) the first approach involves using the macrocycle as a platform capable of carrying different types of ligands, which can be grafted onto either the upper or lower part of the macrocycle. (ii) The second approach relies on the chelating ability provided by the phenolic functions located near the oxidized or non-oxidized sulfur atoms. In the case of the molecular system $[Mn_4(ThiaSO_2)_2F]^-$, the phenolic functions must be preserved. In this context, increasing delocalization along the phenolic units can be achieved either by directly synthesizing the macrocycle with a pre-modified phenol, such as phenylthiacalixarene,[18] or by subsequently modifying the lipophilic part of the thiacalixarene.[25,26] The target ligand, (phenylethynyl)sulfonylcalix[4]arene, cannot be synthesized *via* the cyclocondensation of four 4-(phenylethynyl)phenol groups due to the harsh conditions required for this synthesis (alkaline medium, high temperature, and H_2S atmosphere). Therefore, a synthetic route starting from *p-tert*-butylthiacalixarene had to be developed. The reaction scheme followed to obtain (phenylethynyl)sulfonylcalix[4]arene is described in Fig. 2. This synthetic route enables the preparation of a sulfonylcalixarene modified on its lipophilic moiety while preserving its phenolic groups. For paThiasO_2, the multi-step synthesis (Fig. 2) starting from *p-tert*-butylthiacalixarene (ThiaS) encountered two major obstacles. The first was the protection of the phenolic groups (Fig. 3, step c), to neutralize the complexing power of the macrocycle towards the palladium and copper salts used in the Sonogashira coupling between phenylacetylene and tetra-bromo-thiacalixarene. The second obstacle was the oxidation of sulfur atoms to sulfonyl groups. Acetylation of the phenolic groups proved to be the most reasonable choice for both the protection and deprotection steps of phenolic alcohols. The oxidation step could only be performed out before the deprotection of the acetyl groups and under mild and controlled oxidation conditions to prevent the oxidation of the already formed ethynyl function. It is noteworthy that the formation of sulfonyl groups completely deactivates the macrocycle for the Sonogashira coupling, thus necessitating the coupling prior to oxidation.

The polynuclear complexes $K[Mn_4(ThiaSO_2)_2F]$ (**1**),[17] and $NBu_4[Mn_4(ThiaSO_2)_2F]$ (**2**) were synthesized by a solvothermal method at 170 °C by mixing 1 equivalent of the macrocycle with 5 equivalents of Mn^{2+} in a methanol/water mixture [10 : 1], in the presence of 6 equivalents of a fluorinated salt (either KF or NBu_4F) acting both as a base and as a μ4-bridging ligand. The products for these two syntheses were recovered as pale yellow single crystals and exhibited strong orange eye-perceived luminescence upon a 400 nm laser pointer beam. The same solvothermal procedure, but this time with the macrocycle paThiaSO_2, yielded a non-luminescent powder and the characterization did not allow to conclude on the possible formation of a major complex. Irradiation of the same reaction mixture under microwave (900 W, 30 s) produced a non-crystalline powder (**3**) exhibiting luminescence at room temperature (Fig. 3). Mass spectrometric analysis of this powder, freshly dissolved in dimethylformamide (DMF), shows the presence of the anion $[Mn_4(paThiaSO_2)_2F]^-$, indicating that the complex K $[Mn_4(paThiaSO_2)_2F]$ (**3**) has indeed been formed. Several attempts were made to recrystallize this powder without success in crystallizing the desired compound. Finally, the $[Mn_4(paThiaSO_2)_2F]^-$ complex was isolated as a single crystal by replacing the K^+ counter-anion with tetrabutylammonium (NBu_4^+). The compound $NBu_4[Mn_4(paThiaSO_2)_2F]$ (**4**) is obtained either by solvothermal reaction, mixing paThiaSO_2 and $MnCl_2{\cdot}4H_2O$ in the presence of NBu_4F in a mixture of DMF and methanol in a closed reactor at 110 °C, or by recrystallization of the complex (**3**) in a methanol/DMF mixture in the presence of NBu_4F at 110 °C. According to the HSAB theory, it seems that increasing the affinity between $[Mn_4(paThiaSO_2)_2F]^-$ and the counteranion, namely NBu_4^+, stabilizes the intimate ion pair $NBu_4[Mn_4(paThiaSO_2)_2F]$ in

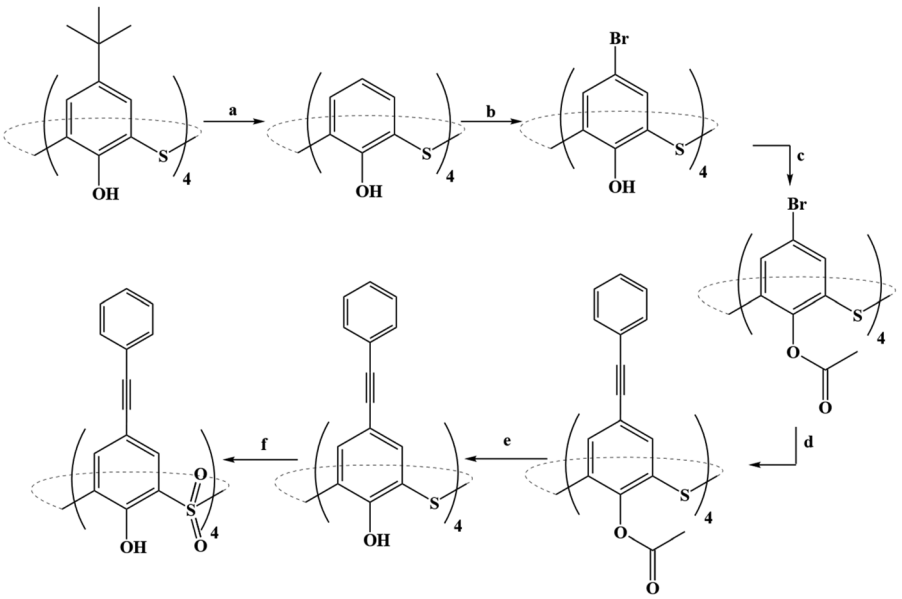

Fig. 2 The reaction scheme for the preparation of paThiaSO$_2$. (a) Phenol/AlCl$_3$, toluene, 72%. (b) *N*-Bromosuccinimide, acetone, 71%. (c) NaOAc, O(Ac)$_2$, 70 °C, 88%. (d) Phenylacetylene, PdCl$_2$(PPh$_3$)$_2$, CuI, Et$_3$N, THF, 85%. (e) NaOH, THF/MeOH, 82%. (f) NaBO$_3$·4H$_2$O, CH$_3$COOH/H$_2$O$_2$, CHCl$_3$, 72%.

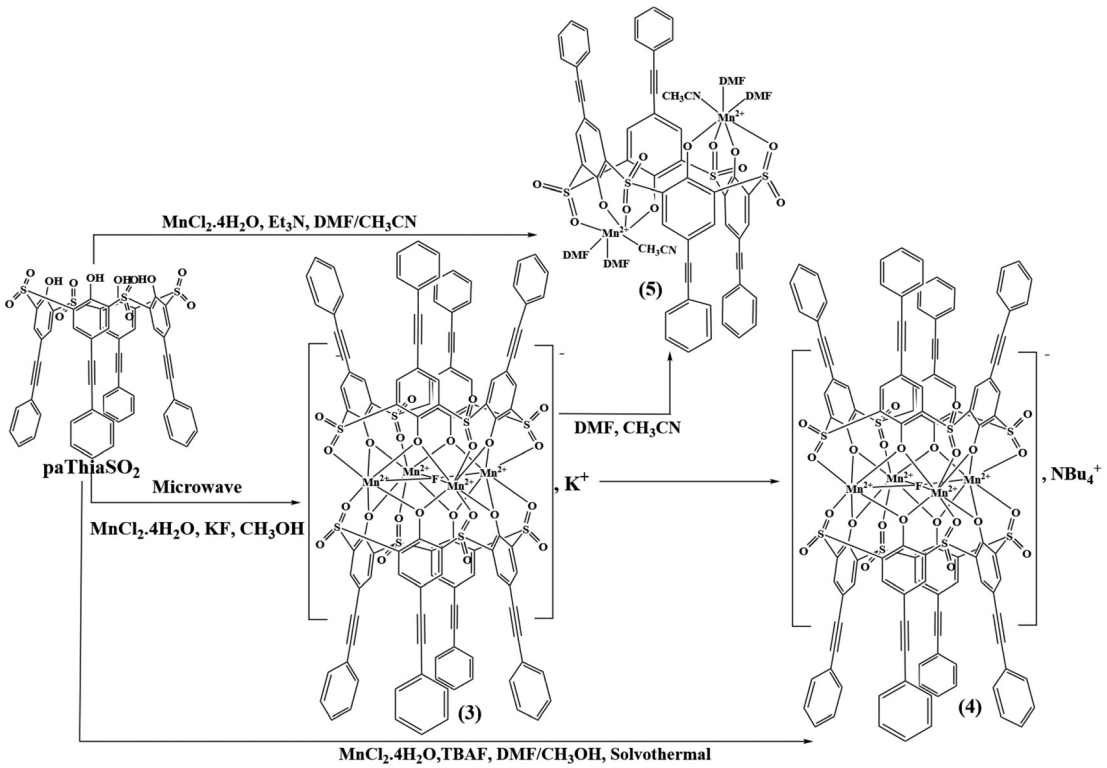

Fig. 3 Reaction scheme for the preparation of the complexes [Mn$_2$(paThiaSO$_2$)(DMF)$_4$(CH$_3$CN)$_2$] (**5**) and NBu$_4$[Mn$_4$(paThiaSO$_2$)$_2$F] (**4**).

solution and thus promotes its crystallization. In addition, vapor-phase acetonitrile diffusion into a solution of (**3**) dissolved in DMF allowed crystallization of the neutral dinuclear complex [Mn$_2$(paThiaSO$_2$)(DMF)$_4$(CH$_3$CN)$_2$] (**5**). This dinuclear complex is more easily formed by reacting paThiaSO$_2$ with MnCl$_2$·4H$_2$O in the presence of triethylamine in DMF and then

crystallizing by acetonitrile diffusion. Previous studies have shown that the complex $[Mn_4(ThiaSO_2)_2F]^-$ is unstable in solution to light and to highly coordinating solvents such as DMF or DMSO, resulting in the formation of an analogous dinuclear complex $[Mn_2(ThiaSO_2)(DMF)_4(H_2O)_2]$.[19]

2.2. Crystal structure

The structure of complex (**1**) has been discussed in previous articles.[17] Compounds (**2**) and (**4**), like compound (**1**), consist of squares of four manganese(II) ions sandwiched between two $ThiaSO_2$ macrocycles, as shown in Fig. 4. In the center of the square formed by the four manganese(II) ions, the presence of μ_4-F^- confers a negative charge to the cluster. The electroneutrality of the complex is achieved by the presence of the cation K^+ for (**1**) and (**3**), or NBu_4^+ for (**2**) and (**4**). The originality of this type of aggregate lies in the peculiar coordination of the Mn^{2+} ions, which are located in the center of a capped trigonal biprism with C_{2v} symmetry. We also note a relatively unusual square plane coordination of the fluoride anion μ^4. Among these three different complexes, the interatomic distances between the Mn^{2+} ions and the oxygen atoms of the coordination sphere do not show any major variations. In complexes (**1**), (**2**) and (**4**), a center of symmetry is located on the fluorine atom. Thus, the two macrocycles sandwiching the manganese ions are perfectly identical. However, for (**1**), the macrocycles adopt a cone conformation, whereas for (**2**) and (**4**), the conformation is a pinched cone. Between (**2**) and (**4**), it is (**2**) that has the most pinched cone conformation (Fig. S1).

In compound (**1**), the cation K^+ is coordinated by sulfonyl and methanol groups. In compound (**2**), the shortest interaction distance between the $[Mn_4(paThiaSO_2)_2F]^-$ anion and NBu_4^+ is 4.553 Å. This interaction occurs between the oxygen of a phenoxy group and the nitrogen atom of the NBu_4^+ cation (Fig. S1). These alternating anions and cations form chains along the *a*- and *b*-axes (Fig. 5). The *ab*-planes formed by these chains are stacked along the *c*-axis with only weak van der Waals-type interactions. In compound (**4**), the shortest interaction distance between the $[Mn_4(paThiaSO_2)_2F]^-$ anion and NBu_4^+ is 4.027 Å. This interaction takes place between an oxygen of a sulfonyl group and the nitrogen atom of the NBu_4^+ cation (Fig. S2). The ion pairs $\{[Mn_4(paThiaSO_2)_2F]^-; NBu_4^+\}$ are assembled in the *ab*-plane by ionic interactions between the oxygen of the sulfonyl groups of the macrocycle and the nitrogen atoms of the NBu_4^+ cation. The *ab*-planes are stacked by introducing a phenylethynyl moiety into the cavity of a macrocycle belonging to another layer (Fig. S3). Two macrocycles are interlocked one inside the other by the π-interaction between two phenylethynyl moieties (shortest distance 3.469 Å). The torsion angles for the four different phenylethynylphenolic units are 50.8°, 3.7°, 64.8° and 36.1°.

The dinuclear complex (**5**) consists of a $paThiaSO_2$ macrocycle adopting a 1,2-alternate conformation and coordinating two Mn^{2+} ions. The coordination sphere of each Mn^{2+} ion is completed by two DMF molecules and one acetonitrile molecule. The coordination of the two Mn(II) ions is perfectly equivalent due to the presence of an inversion center at the center of the complex. The $[MnO_5N_1]$ coordination sphere exhibits a distorted octahedral geometry. The interatomic distances are 2.115(2) Å and 2.109(2) Å for Mn–O_{phenol}, 2.240(2) Å for Mn–$O_{sulfonyl}$, 2.249(3) Å for Mn–$N_{acetonitrile}$, and 2.150(3) Å and 2.198 (3) Å for the Mn–O_{DMF} bond lengths. The torsion angles for the two different phenylethynylphenol units are 31.8° and 15.60°.

2.3. Photophysical characterization

Absorption in DMF solution. Fig. 6 shows the absorption spectra at room temperature in DMF solution of K

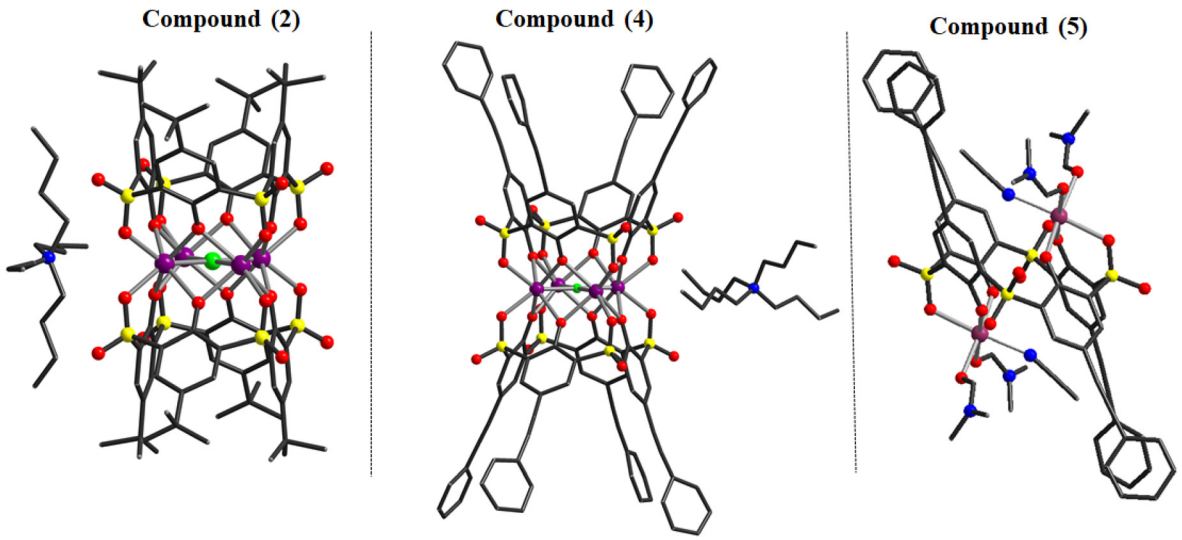

Fig. 4 X-ray structures of compounds (**2**) (a), (**4**) (b) and (**5**) (c). For compounds (**2**) and (**4**), the $ThiaSO_2$ and $paThiaSO_2$ macrocycles adopt a cone conformation and Mn(II) ion assumes a capped biprism trigonal geometry. For compound (**5**), the $paThiaSO_2$ macrocycle adopts a 1,2-alternate conformation and Mn(II) ions assume a distorded octahedral geometry. Atoms are depicted as follows: Mn (purple), O (red), S (yellow), C (grey), F (light green) and N (blue). Hydrogen atoms are omitted for clarity.

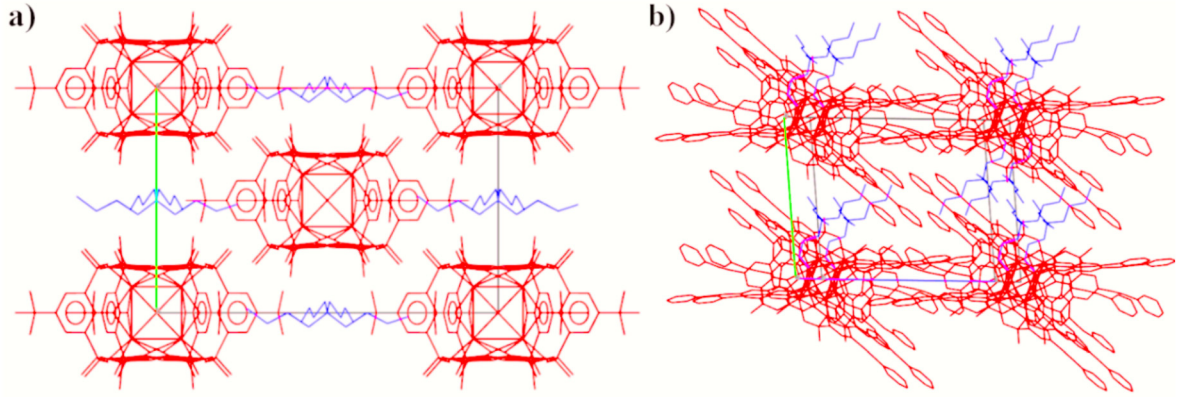

Fig. 5 (a) Packing of compound (**2**), projection along the *c*-axis. (b) Packing of compound (**4**), projection along the *a*-axis. The complexes $[Mn_4(ThiaSO_2)_2F]$ and $[Mn_4(paThiaSO_2)_2F]$ are represented in red, and the NBu_4^+ cation in blue.

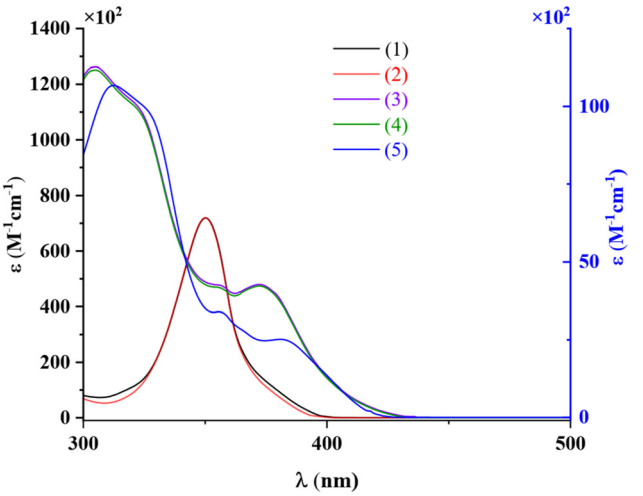

Fig. 6 Absorption spectra in DMF solution of compounds (**1**), (**2**), (**3**), (**4**) and (**5**) at room temperature, $c = 4.07 \times 10^5$ M for (**1**), $c = 4.2 \times 10^5$ M for (**2**), $c = 2.4 \times 10^5$ M for (**3**), $c = 2.38 \times 10^5$ M for (**4**) and $c = 2.98 \times 10^4$ M for (**5**). The left ordinate scale corresponds to compounds (**1**) to (**4**), and the right ordinate scale corresponds to compound (**5**).

$[Mn_4(ThiaSO_2)_2F]$ (**1**), $(NBu_4)[Mn_4(ThiaSO_2)_2F]$ (**2**), K $[Mn_4(paThiaSO_2)_2F]$ (**3**), $(NBu_4)[Mn_4(PaThiaSO_2)_2F]$ (**4**) and $[Mn_2(paThiaSO_2)(DMF)_4(CH_3CN)_2]$ (**5**) between 300 and 450 nm. The absorption spectrum of (**1**) is identical to that of (**2**). The observed absorption bands are mainly the signature of the $ThiaSO_2$ ligand. It can easily be hypothesized that at this concentration the complexes (**1**) and (**2**) are present as free ion pairs, and thus the cation, K^+ for (**1**) and NBu_4^+ for (**2**), has no influence on the absorption. The band can be attributed to π–π* transitions of the $ThiaSO_2$ ligand. The molar extinction coefficient of the intense absorption band at 350 nm is within experimental accuracy identical for the two compounds with a value of ε_{max} = 72 000 M^{-1} cm^{-1}. The absorption spectra of compounds (**3**) and (**4**) show four absorption maxima at 305 nm (ε = 125 135 M^{-1} cm^{-1}), 321 nm (ε = 112 140 M^{-1} cm^{-1}), 356 nm (ε = 46 780 M^{-1} cm^{-1}), and 373 nm (ε = 47 360 M^{-1} cm^{-1}). The profiles of the first three bands (ε_{max} at 305, 321, and 356 nm) correspond to those already described in the literature for the calixarene macrocycle family or for phenyleneethynylene monomers.[22] The band ε_{max} at 373 nm is attributed to the $ThiaSO_2$ macrocycle backbone. It is shifted by 23 nm compared to the complexes (**1**) and (**2**) and its molar extinction coefficient decreases. For compound (**5**), the spectral profile is identical to that of compounds (**3**) and (**4**). However, a red shift of 10 nm is observed for the absorption maxima of compound (**5**). The molar absorption coefficients are about ten times lower than those observed for compounds (**3**) and (**4**).

Solid-state excitation and emission spectra

One-photon excitation. The Stokes excitation and emission spectra in the solid-state at room temperature for compounds (**1**), (**2**), (**3**), and (**4**) are shown in Fig. 7. The one-photon excitation spectral profiles for compounds (**1**) and (**3**) are similar, with maxima at 400 nm and 422 nm, respectively. The excitation spectral profiles of compounds (**2**) and (**4**) are also similar. They exhibit multiple maxima at 326 nm, 370 nm and 412 nm for compound (**2**) and at 339 nm, 366 nm and 414 nm for compound (**4**). All compounds exhibit an intense symmetric emission band centered at 600 nm (**1**), 615 nm (**2**), 645 nm (**3**) and 660 nm (**4**). In all cases, this orange-red emission band originates from the $^4T_1 \rightarrow {}^6A_1$ transition of Mn (II) in a high-spin d^5 configuration. The functionalization of sulfonylcalixarene with phenylethynyl units induces a bathochromic shift of 50 nm in the absorption bands, shifting the excitation threshold from 450 nm for compounds (**1**) and (**2**) to about 500 nm for compounds (**3**) and (**4**). A similar shift is observed in the emission maxima, indicating a change in photophysical properties. The spectroscopic variations reflect a sensitivity to the nature of the cation present, with a clear distinction between the complexes formed with potassium ion (K^+) and those with tetrabutylammonium (NBu_4^+). This differentiation is supported by measurements carried out under aerobic and anaerobic conditions, highlighting the influence of the environment on the electronic behavior of the studied systems.

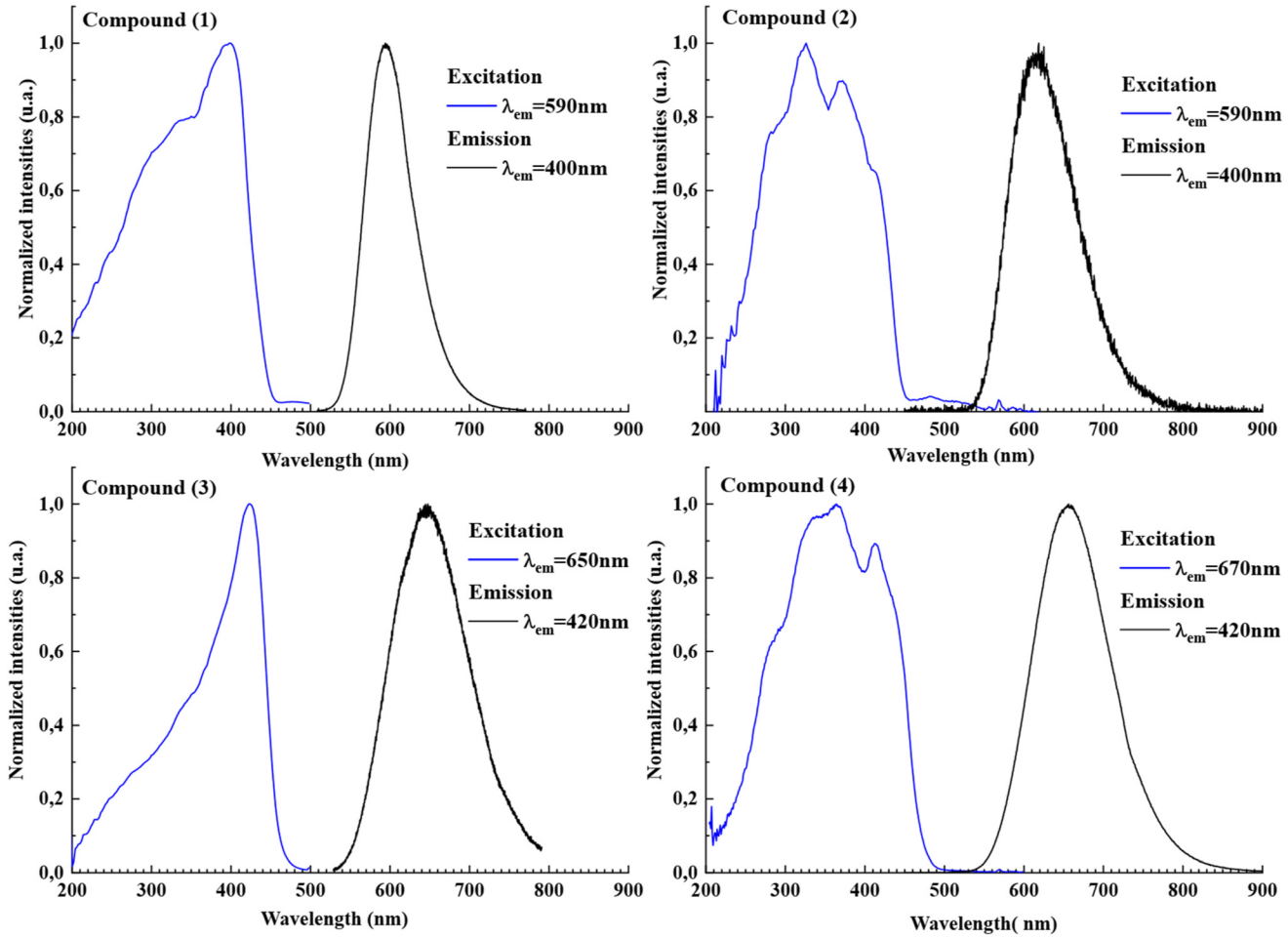

Fig. 7 Solid-state excitation (blue line) and emission (black line) spectra of compounds (**1**), (**2**), (**3**), and (**4**), at room temperature and under air.

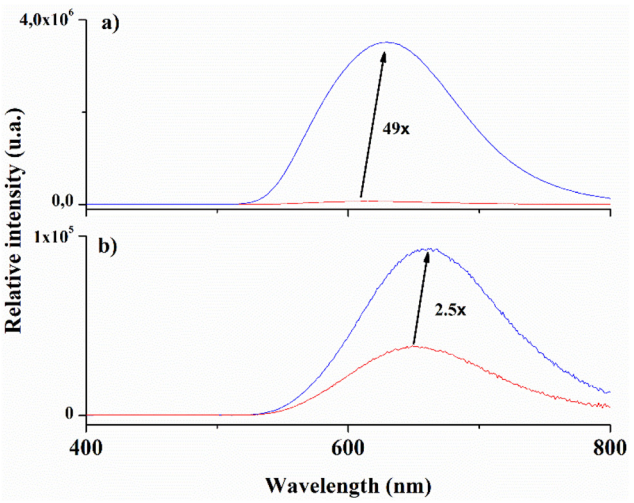

Fig. 8 Solid-state emission spectra of compounds (**2**) (a) and (**4**) (b) upon excitation at 330 nm at room temperature, under air (red line) and vacuum (blue line) conditions.

Fig. 8 exhibits the emission spectra under Stokes excitation in air and under vacuum for compounds (**2**) and (**4**), with tetrabutylammonium as the counteranion. In contrast to compound (**1**), complexes (**2**) and (**4**) show luminescence that is highly sensitive to the presence or absence of oxygen, being 49 times and 2.5 times higher, respectively, in the absence of O_2. At room temperature, the lifetimes of (**2**) are 1.84 ms in vacuum and 0.68 ms in air, while those of (**4**) are 0.68 ms (vacuum) and 0.23 ms (air), respectively. These emission lifetimes are shorter than the lifetime measured in air for compound (**1**), which is 1.63 ms. Fig. S4 shows the evolution over time of the luminescence intensity of the compounds (**2**) and (**4**), starting from air and then exposed to a vacuum. Compound (**4**) responds significantly faster than compound (**2**), reaching its maximum emission intensity after a few seconds. However, the emission intensity of the compound (**2**) shows a remarkable increase under vacuum. This difference is probably due to a slower oxygen desorption rate in the structure of (**2**). Several effects may be responsible for these results: (i) the energy levels of the triplet states of the luminescent anionic complex, as well as the spin–orbit coupling, may be influenced by the iono-covalent character of the cation–anion

interaction; (ii) a change in the rigidity and lattice vibrations may also play a role. Such modifications promote the diffusion of molecular oxygen and enhance the coupling between the electronic levels of the luminescent entity and those of oxygen. In the case of these complexes, the origin of the phenomenon could be a combination of both effects, with a predominant role attributed to oxygen diffusion processes. The structures containing the NBu_4^+ cation show significantly weaker interactions between the anion and the cation, as well as lower densities (1.393 g cm^{-3} for compound (**2**), 1.392 g cm^{-3} for compound (**4**), compared to 1.51 g cm^{-3} for compound (**1**)). Among complexes (**1**), (**2**), and (**4**), complex (**2**) has the largest distance between the nitrogen atom of Bu_4N^+ and the oxygen of a sulfonyl group with $d_{N^+\text{-}OS}$ = 4.87 Å (for (**4**), $d_{N^+\text{-}OS}$ = 4.027 Å, and for (**1**), $d_{K^+\text{-}OS}$ = 2.7 Å).

The excitation and emission measurements for the dinuclear compound (**5**) as a function of temperature, in the presence and absence of O_2, are shown in Fig. S5 and S6. The solid-state emission spectrum of (**5**) exhibits a broad band centered at around 725 nm under a photo-excitation at 325 nm at ambient pressure. To avoid oxygen (O_2)-induced quenching, the luminescence was measured in a vacuum cavity and the maximum emission band increased by 20%. The solid-state emission has also been measured at variable temperature (77–300 K) under excitation at 325 nm in an inert atmosphere (N_2) (Fig. S6). The luminescence increased by 96% (Fig. S5), and the emission maximum shifted by 20 nm from 723 nm to 743 nm from 300 K to 77 K. The emission of complex (**5**) is very weak and, unlike compounds (**1**) to (**4**), is not visible to the naked eye. It is sensitive to oxygen quenching and to temperature. In contrast to the previously reported analogous dinuclear complexes, the replacement of *tert*-butyl functions, such as in the complex $[Mn_2(ThiaSO_2)(DMF)_4(H_2O)_2]$,[19] by phenyl or phenylethynyl groups, such as in the complexes $[Mn_2(ppThiaSO_2)(DMF)_6]$ ($ppThiaSO_2$ = *p*-phenylsulfonylcalix[4]arene)[18] and $[Mn_2(paThiaSO_2)(DMF)_4(CH_3CN)_2]$ (**5**), respectively, had significant effects on the photophysical properties of the complex. The emission of the latter two complexes is weaker and red-shifted compared to the former. These effects are consistent with the observation that the absorption

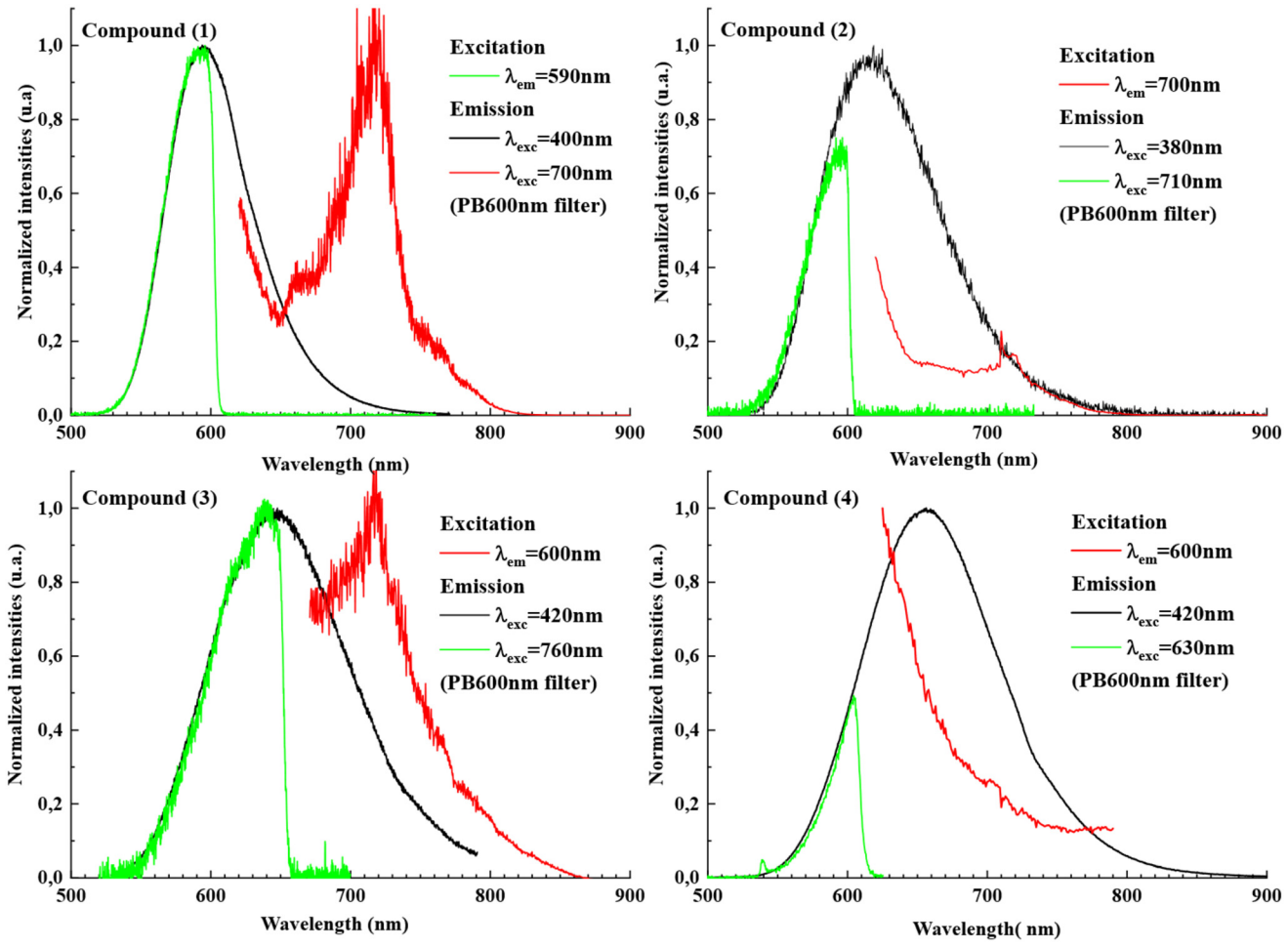

Fig. 9 Solid-state excitation and emission spectra of compounds (**1**), (**2**), (**3**) and (**4**) at room temperature and under air. In red are the two-photon excitation spectra and in green the resulting emission spectra (anti-Stokes) of compounds (**1**) to (**4**). The emission was measured with a 600 nm low-pass filter, which explains the cutoff in the spectra. In black are the emission spectra under one-photon excitation (Stokes).

decreases from $ThiaSO_2$ to $ppThiaSO_2$ and $paThiaSO_2$ macrocycles, which act as antennas.

Two-photon excitation. The anti-Stokes excitation and emission spectra, in the solid-state at room temperature, for compounds (**1**) to (**4**) are shown in Fig. 9. All the anti-Stokes excitation emission spectra show an emission band corresponding to that obtained under Stokes excitation. This shows that all the presented complexes can be excited by two-photon absorption. This confirms that sulfonylcalixarene is a remarkable antenna for sensitizing Mn^{2+} ions through both one- and two-photon excitation. Among the four compounds, compounds (**1**) and (**3**) exhibit the largest two-photon excitation band around 720 nm. The anti-Stokes excitation spectrum of compound (**2**) shows a weak two-photon excitation band, while compound (**4**) shows none. As in the case of one-photon absorption, the replacement of the K^+ counterion by NBu_4^+ induces the most significant change in the photophysical properties of this molecular system.

The room temperature emission lifetime measurements (Stokes and anti-Stokes) of compounds (**1**) to (**4**) in air are shown in Fig. S7. Compound (**1**) exhibits a nearly monoexponential luminescence decay with a calculated lifetime of τ = 1.74 ms. This lifetime is in agreement with previously reported values for the same compound.[16] Compound (**2**) shows a biexponential luminescence decay with τ_1 = 0.0153 ms (85%) and τ_2 = 0.85 ms (15%). The first decay is attributed here to luminescence quenching caused by the presence of oxygen. The lifetimes for compounds (**3**) and (**4**) show multiexponential decay curves, with average lifetimes of τ = 0.091 ms and τ = 0.076 ms, respectively.

The luminescence results confirm that the molecular system $[Mn_4(ThiaSO_2)_2F]^-$ has the ability to be excited by either one-photon or two-photons. However, the functionalization of the system with phenylethynyl chains only resulted in a shift in the Stokes wavelengths of both excitation and emission for the system, without improving the nonlinear absorption. The increased electron delocalization along the phenolic moieties seems to destabilize the electronic delocalization of the thiacalixarene crown, thereby reducing the two-photon absorption capacity of this molecular system. Optical measurements also revealed the important role of the interactions between the cation and the luminescent anion, especially with respect to energy transfer to molecular oxygen.

3. Conclusion

Thiacalixarene complexes have been studied since the late 1990s when this macrocycle was first synthesized. The structure of this macrocycle, with its chelating functions formed by phenolic groups located near oxidized or non-oxidized sulfur atoms, immediately showed strong potential for the development of metal complexes. In addition to its role as a highly structuring ligand for the formation of polynuclear complexes, thiacalixarene exhibits interesting electronic properties that allow it to efficiently sensitize Mn^{2+} ions. Tetranuclear complexes based on Mn^{2+} ions and sulfonylcalixarene macrocycles exhibit, when excited with blue light (360 to 400 nm), a broad luminescence band around 600 nm, resulting from the d–d transition $T_1(t_2g^4eg^1) \rightarrow {}^6A_1(t_2g^3eg^2)$ of the Mn^{2+} ions. To broaden the applications of these luminescent complexes, their ability to be excited by lower energy multiphoton absorption was investigated. Previous nonlinear optics studies had highlighted the interesting properties of this macrocycle when functionalized with phenylethynyl groups. Various complexes based on *p-tert*-butylsulfonyl[4]arene and *p*-phenylethynylsulfonylcalix[4]arene macrocycle derivatives have been synthesized and characterized. The results obtained demonstrate the possibility of two-photon sensitization of Mn^{2+} ions through the sulfonylcalixarene macrocycle. However, increasing electronic delocalization along the phenolic units negatively affects the anti-Stokes excitations properties of these molecular systems. Depending on the nature of the counteranion (NBu_4^+ or K^+), the luminescence of the Mn^{2+} ions can be quenched more or less intense. The most probable mechanism is an energy transfer from the excited complex to O_2, thereby exciting O_2 from its ground state $^3\Sigma\_g^-$ to its excited state $^1\Sigma\_g^+$.[27,28] The quenching is more effective when the interaction between the tetrabutylammonium and the sulfonyl groups is weaker and when the open structure facilitates the diffusion of O_2 within the crystalline network. This work contributes to a better understanding of the sulfonylcalixarene/Mn^{2+} luminescent systems. It also provides a way to functionalize the upper rim of the macrocycle to increase electron delocalization along the phenolic units while preserving the complexing nature of the phenolic functions. Further studies are underway to explore and better understand the sensitivity of this type of system to oxygen.

4. Experimental

All chemicals and solvents were used as received (solvents and chemicals: Aldrich); *p-tert*-butylthiacalix[4]arene (*p-tert*-ThiaS),[29] thiacalix[4]arene (ThiaS), *p-tert*-butylsulfonylcalix[4]arene ($ThiaSO_2$),[30] *p*-bromo-thiacalix[4]arene (ThiaSBr)[31] and K $[Mn_4(ThiaSO_2)_2F]$ (**1**)[17] were synthesized using the protocols from the literature.

4.1 Synthesis of *p*-bromo-acetoxythiacalix[4]arene (ThiaSBrOAc)

Under inert atmosphere, ThiaSBr (4.9 g, 6 mmol) is suspended in acetic anhydride (50 ml), and anhydrous sodium acetate (10 g) is added. The solution is refluxed for 24 hours and then hydrolyzed for 1 hour after returning to room temperature. The powder is filtered under vacuum and rinsed with methanol. After drying, the *p*-bromo-acetoxythiacalix[4]arene is used without purification for the next step. Yield = 88%. RMN ^1H (Fig. S8, $CDCl_3$, 300 MHz, 293 K): δ (ppm) = 7.9 (d, 4H, J = 4.64 Hz, $H_{1,3}$–Ar), 7.69 (d, 2H, J = 2.35 Hz, $H_{1,3}$–Ar), 7.19 (d, 2H, J = 2.29 Hz, $H_{1,3}$–Ar), 2.55 (s, 3H, ArO–$COCH_3$), 2.41 (s, 6H, ArO–CO–CH_3), 1.71 (s, 3H, ArO–CO–CH_3). MS (ESI): m/z = 1002.6 $[M + Na]^+$. IR: ν (cm^{-1}) = 3058, 2362, 2332, 2284, 2172, 2106, 1906,

1768, 1546, 1414, 1366, 1170, 1112, 1078, 1042, 1010, 900, 876, 834, 792, 762, 690, 632. Melting point: 354 °C.

4.2 Synthesis of *p*-phenylacetylene-acetoxythiacalix[4]arene (paThiaSOAc)

Under inert atmosphere, ThiaSBrOAc (0.74 g, 0.75 mmol) is dissolved in anhydrous THF (15 ml), followed by the addition of triethylamine Et_3N (0.45 ml). To this solution $PdCl_2(PPh_3)_2$ (0.052 g, 0.074 mmol), CuI (0.002 g, 0.007 mmol), and phenylacetylene (0.45 ml, 4.1 mmol) are added successively. The solution turns dark orange. The reaction mixture is heated to 40 °C for 48 hours. The solution is then evaporated to dryness. The product obtained is dissolved in 50 ml of dichloromethane and washed with 2 × 25 ml of HCl (1 M). The organic phase is dried with Na_2SO_4 and concentrated. The addition of methanol allows the precipitation of a white powder of paThiaSOAc. After filtration and drying, paThiaSOAc is obtained with a yield of 85%. RMN ^{1}H (Fig. S9, $CDCl_3$, 300 MHz, 293 K): δ (ppm) = 7.66 (s, 8H, $H_{1,3}$–Ar), 7.5 (dd, 8H, J = 2.95, 6.66 Hz, $H_{10,14}$–Ar), 7.36 (m, 12H, H_{11-13}–Ar), 1.83 (s, 12H, ArO–COH_3). MS (ESI): m/z = 1087.1 $[M + Na]^+$. IR: ν (cm^{-1}) = 3062, 2360, 2328, 1770, 1600, 1572, 1492, 1434, 1368, 1172, 1080, 1010, 894, 818, 802, 757, 688, 626. Melting point: 310 °C.

4.3 Synthesis of *p*-phenylacetylenethiacalix[4]arene (paThiaS)

paThiaSOAc (0.5 g, 0.47 mmol) is suspended in 20 mL of THF and 6 mL of a concentrated sodium hydroxide solution (8 M, THF (4 ml)/methanol (2 ml)) is added. The solution is heated under reflux for 4 hours until the powder is completely dissolved. The solution is evaporated to dryness and the product is redissolved in 20 mL chloroform, then washed with 2 × 10 mL HCl (1 M). The organic phase is dried over $MgSO_4$ and then evaporated to dryness. The product is taken up in ether and precipitated with stirring. After filtration and drying, paThiaS is obtained with a yield of 82%. RMN ^{1}H (Fig. S10, $CDCl_3$, 300 MHz, 293 K): δ (ppm) = 9.29 (d, 4H, J = 3.09 Hz, Ar–OH), 7.83 (s, 8H, H–Ar), 7.5 (m, 8H, H–Ar), 7.32 (m, 12H, H–Ar). RMN ^{13}C ($CDCl_3$, 100 MHz, 293 K): δ (ppm) = 157.8 (Ar, C5), 142.2 (Ar, C1,3), 131.6 (Ar, C10,14), 128.5 et 128.4 (Ar, C_{11-13}), 122.8 (Ar, C9), 120.6 (Ar, C4,6), 117.4 (Ar, C2), 89.8 (C≡C, C7), 87.1 (C≡C, C8). MS (ESI): m/z = 895.1 $[M - H]^-$. IR: ν (cm^{-1}) = 3316, 3054, 2258, 2336, 1770, 1598, 1578, 1550, 1492, 1446, 1386, 1342, 1314, 1260, 1236, 1176, 1156, 1074, 1026, 892, 814, 752, 688. Melting point: 215 °C.

4.4 Synthesis of *p*-phenylacetylenesulfonylcalix[4]arene (paThiaSO$_2$)

In a 10 ml flask, 0.2 g of paThiaS (0.22 mmol) is dissolved in 0.4 mL of chloroform. To this solution, 3 mL of acetic acid, 1 mL of hydrogen peroxide (30%) and 0.38 g of sodium perborate tetrahydrate $NaBO_3{\cdot}4H_2O$ (2.5 mmol) are added. The solution was stirred for 16 hours at room temperature. Then, 10 mL of HCl (1 M) and 10 mL of chloroform are added to the reaction medium for extraction. The organic phase is extracted, washed with 10 mL HCl (1 M) and dried over $MgSO_4$. The resulting solution is evaporated to dryness. The product is taken up in ether and precipitated with stirring. After filtration and drying, paThiaSO$_2$ is obtained with a yield of 72%. RMN ^{1}H (Fig. S11, DMSO-d_6, 300 MHz, 293 K): δ (ppm) = 8.14 (s, 8H, $H_{1,3}$–Ar), 7.51 (m, 8H, $H_{10,14}$–Ar), 7.35 (m, 12H, H_{11-13}–Ar). RMN ^{13}C (DMSO-d_6, 100 MHz, 293 K): δ (ppm) = 137.3 (Ar, C5), 132.4 (Ar, C1,3), 131.2 (Ar, C10,14), 129.87 (Ar, C4,6), 128.3 (Ar, C_{11-13}), 121.9 (Ar, C9), 89.5 (C≡C, C7), 86.6 (C≡C, C8). MS (ESI): m/z = 1023.1 $[M - H]^-$. IR: ν (cm^{-1}) = 3456, 2958, 2924, 2853, 2363, 1591, 1494, 1468, 1411, 1384, 1267, 1197, 1166, 1136, 1080, 1037, 932, 910, 799, 756, 715, 690, 616. Melting point: 230 °C.

4.5 Synthesis of $NBu_4[Mn_4(ThiaSO_2)_2F]$ (2)

In a Teflon autoclave of 20 mL were added ThiaSO$_2$ (0.05 g, 0.06 mmol), $MnCl_2{\cdot}4H_2O$ (0.05 g, 0.3 mmol), and tetra-*n*-butylammonium fluoride hydrate (TBAF) (0.1 g, 0.38 mmol anhydrous basis). The reactants were dissolved in a solvent mixture of MeOH/H_2O (10/0.5 in mL). After heating for two days in an oven at 170 °C, long needle-like crystals of compound (**2**) were isolated, washed several times with methanol, and dried (yield = 74%). Elemental analysis (mass%): $C_{96}H_{124}F_1N_1Mn_4O_{24}S_8$ (2171.26 g mol^{-1}): calc Mn 10.12, S 11.81; found Mn 10.05, S 11.72. IR ν (cm^{-1}) = 3443, 2959, 2870, 1604, 1517, 1462, 1364, 1331, 1265, 1220, 1196, 1136, 1087, 907, 836, 796, 748, 651, 627.

4.6 Synthesis of $K[Mn_4(paThiaSO_2)_2F]$ (3)

paThiaSO$_2$ (0.01 g, 9.76 μmol), $MnCl_2{\cdot}4H_2O$ (0.01 g, 0.05 mmol) and KF (0.02 g, 0.34 mmol) are suspended in 5 mL of methanol. The mixture is heated under a microwave (900 W) for 3 × 30 s. A white powder, which shows an intense red eye-perceived emission under a 400 nm laser pointer, is obtained by centrifugation and rinsed 3 times with 3 mL of methanol. After drying, the light yellow powder of (**3**) is obtained in 32% yield. MS (ESI): m/z = 2278.8 $[M]^-$. IR ν (cm^{-1}) = 3443, 1583, 1492, 1470, 1387, 1338, 1268, 1191, 1128, 1079, 925, 827, 785, 743, 695, 617.

4.7 Synthesis of $NBu_4[Mn_4(paThiaSO_2)_2F]$ (4)

Method 1: In a Teflon autoclave of 10 mL were added paThiaSO$_2$ (0.05 g, 9.76 μmol), $MnCl_2{\cdot}4H_2O$ (0.01 g, 0.05 mmol) and TBAF (0.02 g, 0.34 mmol). The reactants were dissolved in a solvent mixture of DMF/MeOH (0.3/0.5 in mL). After heating for 24 h in an oven at 110 °C and slow cooling (0.1° min^{-1}), needle-like crystals of compound (**4**) were isolated (yield 43%). *Method 2*: In a Teflon autoclave of 10 mL were added 0.03 g of (**3**) and 0.02 g TBAF (0.34 mmol). The reactants were dissolved in a solvent mixture of DMF/MeOH (0.3/0.5 in mL) After heating for 24 h in an oven at 110 °C and slow cooling (0.1° min^{-1}), needle-like crystals of compound (**4**) were isolated, washed several times with methanol, and dried (yieds 34%). Elemental analysis (mass %): $C_{128}H_{92}F_1N_1Mn_4O_{24}S_8$ (2523.36 g mol^{-1}): calc Mn 8.71, S 10.16; found Mn 8.73, S 10.11. MS (ESI): m/z = 2278.8 $[M]^-$. IR ν (cm^{-1}) = 3451, 1590, 1494, 1462, 1384, 1250, 1184, 1136, 1078, 984, 928, 830, 792, 751, 690, 653, 624.

4.8 Synthesis of $[Mn_2(paThiaSO_2)(DMF)_4(ACN)_2]$ (5)

Method 1: 0.01 g (4.1 μmol) of complex (**3**) is dissolved in 0.2 ml of DMF. After slow diffusion of acetonitrile vapor, compound (**5**) is recovered in the form of yellow single crystals (yields 27%). *Method 2*: $paThiaSO_2$ (0.02 g, 0.0196 mmol) and $MnCl_2{\cdot}4H_2O$ (0.01 g, 0.05 mmol) are dissolved in 0.5 ml of DMF. Triethyl amine (20 μl, 0.14 mmol) are added to the solution. After slow diffusion of acetonitrile vapor, compound (**5**) is recovered in the form of yellow single crystals (yields 43%). Elemental analysis (mass%): $C_{72}H_{62}N_6Mn_2O_{12}S_4$ (1441.43 g mol^{-1}): calc Mn 7.62, S 8.9; found Mn 7.64, S 8.11. IR ν (cm^{-1}) = 3437, 2960, 2923, 2853, 2370, 2345, 1591, 1494, 1384, 1322, 1269, 1189, 1158, 1119, 1070, 832, 799, 755, 717.

4.9 Characterizations

Suitable crystals of compounds (**2**), (**4**) and (**5**) were selected and mounted on a Rigaku-OD Synergy-S single-crystal diffractometer equipped with an Hypix-100 detector. Intensities were collected at 100 K with copper radiation (λ = 1.54184 Å) by means of the CrysalisPro software.[32] Reflection indexing, unit-cell parameters refinement, Lorentz-polarization correction, peak integration and background determination were carried out with the CrysalisPro software.[32] An analytical absorption correction was applied using the modeled faces of the crystal.[33] The resulting set of *hkl* was used for structure solution and refinement. The structures were solved with the ShelXT[34] structure solution program using the intrinsic phasing solution method and by using Olex2 [35] as the graphical interface. The model was refined with version 2018/3 of ShelXL[36] using least-squares minimization.

CCDC 2034491 for (**2**), 2425373 for (**4**) and 2430432 for (**5**) contain the supplementary crystallographic data for this paper.

Solid-state excitation and emission spectra were recorded with a commercial fluorimeter (Horiba Jobin Yvon FL3 22, Fluorolog-3) equipped with a Xe lamp 450 W, and a UV Vis near-IR photomultiplier (Hamamatsu R928, sensitivity 190–860 nm). The excitation/emission spectra were realized on powder samples pasted directly onto copper plates using conductive silver glue. Appropriate filters were utilized to remove the laser light, the Rayleigh scattered light, and associated harmonics from the emission spectra. The emission spectra were corrected for the instrumental response function. For the measurements realized at variable temperatures (77 K–300 K), the samples were introduced in an OptistatCF liquid nitrogen-cooled cryostat from Oxford Instruments. Luminescence decays (τ > 10 μs) were also measured at room temperature using this apparatus with a xenon flash lamp (phosphorescence mode). Lifetimes were averaged of 2 or 3 independent determinations. The air pressure-dependent solid-state luminescence spectra were realized in a cryostat equipped with a primary pump.

Stokes emission and excitation spectra (black and blue curves respectively) are made on a home made spectrofluorimeter. A xenon laser-driven light source (EQ99 from Energetiq) is coupled into a Jobin Yvon Gemini double monochromator and used to illuminate the sample over a 2 × 2 mm spot. The emission is then collected by an optical fiber feeding a monochromator (ANDOR KYMERA328i) equipped with an EMCCD camera (ANDOR NEWTON) and a set of order removinf filters. The whole setup has been calibrated by use of a calibrated power meter for the light source (918D from Newport) and by a calibrated lamp (Avantes Avalight-DH-CAL) for the detection.

Anti-Stokes emission and excitation spectra (green and red curves respectively) are performed using an OPO laser (NT-230-50-SH from Ekspla) as the light source and the same detection system as described for Stokes measurement but with the addition of a low pass filter at 600 nm to remove the laser diffusion.

Lifetime were performed using the OPO laser as the excitation source but this time the light is collected by another optical fibre and send to a Jobin Yvon TRIAX330 monochromator coupled with a Peltier cooled R2949 Hamamatsu photomultiplier. The emitted photons are sorted according to their arrival after the laser pulse thanks to an MCS6A multichannel scaler from FastcomTec. The light diffused by the laser is filtered by the monochromator and additional short or high pass filters depending on the conditions of excitation and emission.

Nuclear magnetic resonance. Proton ^1H NMR spectra were recorded on a Bruker AVS 300 (300 MHz) spectrometer. $(CD_3)_2SO$ was used as the intern deuterated reference δ_H (ppm) 2.50.

Mass spectrometer. Mass spectra were recorded on a MicrOTOFD II-Bruker spectrometer with an ElectroSpray Ionization method (ESI), allowing a mass detection between 50 and 20 000 *m*/*z*.

Conflicts of interest

There are no conflicts to declare.

Data availability

Supporting data are included in the supplementary information (SI). Supplementary information: synthesis details, photophysical data, and X-ray crystallography details. See DOI: https://doi.org/10.1039/d5dt02234g.

CCDC 2034491 (**2**), 2425373 (**4**) and 2430432 (**5**) contain the supplementary crystallographic data for this paper.[37a–c]

References

1 O. S. Wenger, *J. Am. Chem. Soc.*, 2018, **140**, 13522–13533.
2 C. Bizzarri, E. Spuling, D. M. Knoll, D. Volz and S. Bräse, *Coord. Chem. Rev.*, 2018, **373**, 49–82.
3 D. M. Arias-Rotondo and J. K. McCusker, *Chem. Soc. Rev.*, 2016, **45**, 5803–5820.

4 C. E. Housecroft and E. C. Constable, *Chem. Soc. Rev.*, 2015, **44**, 8386–8398.
5 F. Heinemann, J. Karges and G. Gasser, *Acc. Chem. Res.*, 2017, **50**, 2727–2736.
6 P. Herr, C. Kerzig, C. B. Larsen, D. Häussinger and O. S. Wenger, *Nat. Chem.*, 2021, **13**, 956–962.
7 Q. Zhou, L. Dolgov, A. M. Srivastava, L. Zhou, Z. Wang, J. Shi, M. D. Dramićanin, M. G. Brik and M. Wu, *J. Mater. Chem. C*, 2018, **6**, 2652–2671.
8 J. P. Harris, C. Reber, H. E. Colmer, T. A. Jackson, A. P. Forshaw, J. M. Smith, R. A. Kinney and J. Telser, *Can. J. Chem.*, 2017, **95**, 547–552.
9 Y. Li, S. Qi, P. Li and Z. Wang, *RSC Adv.*, 2017, **7**, 38318–38334.
10 Enhancement of the Luminescent Properties of a New Red-Emitting Phosphor, $Mn_2(HPO_3)F_2$, by Zn Substitution | Inorganic Chemistry, https://pubs-acs-org.docelec.univ-lyon1.fr/doi/10.1021/ic201226t, (accessed October 21, 2025).
11 M. J. Sumalatha and R. K. Guntu, *Phys. B*, 2025, **715**, 417612.
12 N. R. K. Chand, B. K. Sudhakar, G. Ravikumar, G. S. Rao and C. S. Rao, *Phys. Scr.*, 2021, **96**, 125020.
13 Z. Chen, E. Song, S. Ye and Q. Zhang, *J. Appl. Phys.*, 2017, **122**, 213102.
14 A. V. Artem'ev, M. P. Davydova, A. S. Berezin, V. K. Brel, V. P. Morgalyuk, I. Y. Bagryanskaya and D. G. Samsonenko, *Dalton Trans.*, 2019, **48**, 16448–16456.
15 H. O. Reid, I. Kahwa, A. White and D. Williams, *Inorg. Chem.*, 1998, **37**, 3868–3873.
16 Y. Suffren, N. O'Toole, A. Hauser, E. Jeanneau, A. Brioude and C. Desroches, *Dalton Trans.*, 2015, **44**, 7991–8000.
17 M. Lamouchi, E. Jeanneau, A. Pillonnet, A. Brioude, M. Martini, O. Stéphan, F. Meganem, G. Novitchi, D. Luneau and C. Desroches, *Dalton Trans.*, 2012, **41**, 2707–2713.
18 C. Lecourt, Y. Suffren, E. Jeanneau, D. Luneau and C. Desroches, *Cryst. Growth Des.*, 2022, **22**, 2279–2288.
19 N. O'Toole, C. Lecourt, Y. Suffren, A. Hauser, L. Khrouz, E. Jeanneau, A. Brioude, D. Luneau and C. Desroches, *Eur. J. Inorg. Chem.*, 2019, **2019**, 73–78.
20 E. Brouyère, A. Persoons and J. L. Brédas, *J. Phys. Chem. A*, 1997, **101**, 4142–4148.
21 R. Andreu, S. Franco, J. Garín, J. Romero, B. Villacampa, M. J. Blesa and J. Orduna, *ChemPhysChem*, 2012, **13**, 3204–3209.
22 P. J. A. Kenis, O. F. J. Noordman, S. Houbrechts, G. J. van Hummel, S. Harkema, F. C. J. M. van Veggel, K. Clays, J. F. J. Engbersen, A. Persoons, N. F. van Hulst and D. N. Reinhoudt, *J. Am. Chem. Soc.*, 1998, **120**, 7875–7883.
23 G. Hennrich, M. T. Murillo, P. Prados, H. Al-Saraierh, A. El-Dali, D. W. Thompson, J. Collins, P. E. Georghiou, A. Teshome, I. Asselberghs and K. Clays, *Chem. – Eur. J.*, 2007, **13**, 7753–7761.
24 R. Zieba, C. Desroches, F. Chaput, M. Carlsson, B. Eliasson, C. Lopes, M. Lindgren and S. Parola, *Adv. Funct. Mater.*, 2009, **19**, 235–241.
25 S. Parola and C. Desroches, *Collect. Czech. Chem. Commun.*, 2004, **69**, 966–983.
26 P. Lhoták, *Eur. J. Org. Chem.*, 2004, 1675–1692.
27 R. Q. Albuquerque, Z. Popović, L. De Cola and G. Calzaferri, *ChemPhysChem*, 2006, **7**, 1050–1053.
28 M. S. Khakhalina, O. A. Rodionova and M. V. Puzyk, *Opt. Spectrosc.*, 2009, **106**, 529–531.
29 H. Kumagai, M. Hasegawa, S. Miyanari, Y. Sugawa, Y. Sato, T. Hori, S. Ueda, H. Kamiyama and S. Miyano, *Tetrahedron Lett.*, 1997, **38**, 3971–3972.
30 N. Morohashi, N. Iki, A. Sugawara and S. Miyano, *Tetrahedron Lett.*, 2001, **57**, 5557–5563.
31 C. Desroches, C. Lopes, V. Kessler and S. Parola, *Dalton Trans.*, 2003, 2085–2092.
32 Rigaku Oxford Diffraction, *CrysAlisPro Software System, Version 1.171.40.67a*, Rigaku Corporation, Oxford, UK, 2019.
33 R. C. Clark and J. S. Reid, *Acta Crystallogr., Sect. A: Found. Crystallogr.*, 1995, **51**, 887–897.
34 G. M. Sheldrick, *Acta Crystallogr., Sect. A: Found. Adv.*, 2015, **71**, 3–8.
35 O. V. Dolomanov, L. J. Bourhis, R. J. Gildea, J. A. K. Howard and H. Puschmann, *J. Appl. Crystallogr.*, 2009, **42**, 339–341.
36 G. M. Sheldrick, *Acta Crystallogr., Sect. C: Struct. Chem.*, 2015, **71**, 3–8.
37 (*a*) CCDC 2034491: Experimental Crystal Structure Determination, 2025, DOI: 10.5517/ccdc.csd.cc2691rb; (*b*) CCDC 2425373: Experimental Crystal Structure Determination, 2025, DOI: 10.5517/ccdc.csd.cc2mdsvp; (*c*) CCDC 2430432: Experimental Crystal Structure Determination, 2025, DOI: 10.5517/ccdc.csd.cc2ml21c.